A Lyapunov-Based Magnetorquer-Only Sun-Pointing Controller

Paulo Fisch*
Carnegie Mellon University
5000 Forbes Avenue
Pittsburgh, PA 15217
pfisch@cmu.edu

Pedro Cachim*
Carnegie Mellon University
5000 Forbes Avenue
Pittsburgh, PA 15217
pcachim@andrew.cmu.edu

Max Holliday
NASA Ames Research Center
N-254 Moffett Field
Moffett Field, CA 94035
max.a.holliday@nasa.gov

Rodrigo Ventura
Instituto Superior Técnico
Av. Rovisco Pais 1
1049-001 Lisboa
rodrigo.ventura@isr.tecnico.ulisboa.pt

Pedro Lourenço
GMV
Alameda dos Oceanos 115
1990-392 Lisboa
palourenco@gmv.com

Zachary Manchester
Carnegie Mellon University
5000 Forbes Avenue
Pittsburgh, PA 15217
zacm@cmu.edu

***Abstract*—We present a control scheme that can spin stabilize a spacecraft about its minor or major axis of inertia and simultaneously point this axis at the sun using only magnetorquers and low-cost sensors. The controller is implemented as a switched system, alternating between a spin-stabilizing and a target-pointing control law. Each control law locally minimizes a Lyapunov function. We perform a preliminary stability analysis to evaluate the controller's ability to drive the system to a Lyapunov-stable equilibrium in finite time within defined tolerances for the axisymmetric case. We evaluate our controller's performance through both extensive Monte-Carlo simulations for the axisymmetric and the general tri-inertial case and on orbit as part of the recent PY4 mission. The controller points within fifteen degrees of the sun in less than half an orbit in the PY4 mission and achieves nearly 100% success in numerical simulations.**

TABLE OF CONTENTS

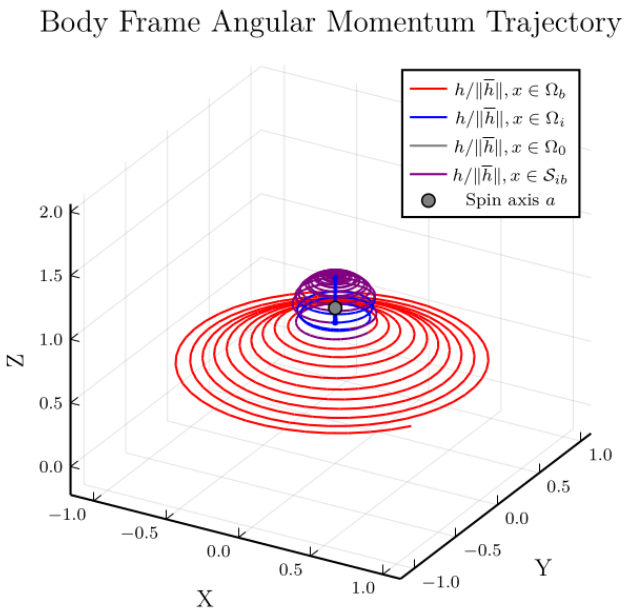

Figure 1. Our Lyapunov-based controller switches behaviors in different parts of the trajectory depending on the value of each component of the Lyapunov function. Red corresponds to spin stabilization, blue corresponds to sun pointing, and purple to the sliding mode/fast switching between the two. This figure considers the axisymmetric case. Note how the controller alternates between the two modes as the angular momentum moves first toward the target spin axis and then toward the Sun vector.

1. INTRODUCTION

Satellites are often reliant on solar power for on-orbit energy generation, which makes maintaining sun pointing critical. Failure of the attitude control system can lead to power starvation and premature mission failure. This motivates the development of "safe-mode" controllers capable of swiftly and efficiently pointing solar panels at the sun while requiring a minimal set of actuators, sensors, and computational resources.

There is extensive literature on the use of magnetorquers as actuators for attitude control. Ovchinnikov and He present two comprehensive surveys of active attitude control methods [1], [2]. Flat-spin recovery and spin-stabilization controllers have been extensively researched for both reaction wheel and magnetorquer actuators [3],[4],[5],[6]. Sun-pointing controllers have been studied since the 1960's [7]. Most of them, however, have low accuracy [8], are designed for reaction wheel actuators [1], or are designed for large satellites and low tumble rates [9].

We address the limitations of previous sun-pointing controllers with a novel Lyapunov-based controller that com-

979-8-3315-7360-7/26/$31.00 ©2026 IEEE

* Both authors had equal contribution to this paper

bines spin stabilization [3] and sun-pointing [10], [11], [12] behaviors into a unified control law to achieve reliable sun-pointing. Our contributions include:

1. A Lyapunov-based magnetorquer-only controller that combines sun-pointing and spin-stabilization behaviors
2. A preliminary stability analysis and progress towards a proof of the ability of the controller to drive the system to a Lyapunov-stable configuration within a positively invariant set bounded by defined distance margins to the target equilibrium
3. Monte-Carlo evaluation of the controller in simulations with realistic hardware parameters
4. On-orbit experimental evaluation of the controller during the PY4 mission [13]

The paper proceeds as follows: We first present related work and background in Section 2, then present the controller and its stability analysis in Section 3. Section 4 presents Monte-Carlo simulations to validate the performance of our controller, then Section 5 presents the results of an on-orbit experimental demonstration on the PY4 CubeSat mission. Finally, we summarize our conclusions and directions for future work in Section 6.

2. BACKGROUND

This section briefly reviews important background on satellite attitude dynamics and Lyapunov stability.

Attitude Dynamics

We model a satellite with magnetorquers as a rigid body governed by Euler's equation [14]:

$$J\dot{\omega} + \omega \times J\omega = \tau, \tag{1}$$

where J is the spacecraft's inertia tensor expressed in body-fixed coordinates, ω is the body-frame angular-velocity vector, and τ is the applied torque (also expressed in the body frame). We also define the angular momentum,

$$h = J\omega, \tag{2}$$

which allows us to re-write (1) as:

$$\dot{h} + \omega \times h = \tau. \tag{3}$$

In the specific case of magnetorquers, the torque is given by,

$$\tau = -b \times \mu = -\hat{b}\mu, \tag{4}$$

where b is the local magnetic field vector of the Earth at the spacecraft's current location in body frame, μ is the magnetic moment vector generated by the spacecraft's actuators in body frame, and $\hat{b}$ denotes the 3×3 skew-symmetric cross-product matrix:

$$\hat{b} = \begin{bmatrix} 0 & -b_3 & b_2 \\ b_3 & 0 & -b_1 \\ -b_2 & b_1 & 0 \end{bmatrix}. \tag{5}$$

The dynamics (1) exhibit some well-known characteristics: There are equilibrium spin states about the three eigenvectors of J, and the equilibria corresponding to the smallest and largest eigenvalues ("minor" and "major" axes, respectively) are stable, while the equilibrium associated with the intermediate axis is unstable [14].

The magnetic field in the body frame exhibits the following dynamic behavior:

$$\dot{b}(t) = b \times \omega + R_i^b \dot{b}_i(t), \tag{6}$$

with R_i^b the rotation matrix from the inertial to the body frame and $\dot{b}_i$ the time derivative of the geomagnetic field in the inertial frame.

We consider additionally the body frame unit direction vector $s \in \mathrm{S}^2$, fixed in the inertial frame, representing the sun/target direction. Its motion will be defined by the nonlinear differential equation (7).

$$\underbrace{\begin{bmatrix} \dot{h} \\ \dot{s} \end{bmatrix}}_{\dot{x}} = \underbrace{\begin{bmatrix} \mu \times b(t) - \omega \times h \\ -\omega \times s \end{bmatrix}}_{f(x,\mu,t)} \tag{7}$$

Lyapunov Stability

The necessary background on Lyapunov Stability for this paper is available in textbooks such as [15] and [16], with content dedicated to switched systems in [17]. We briefly summarize the results most relevant to the proof presented in this paper in this section.

Consider a locally Lipschitz function with an equilibrium at the origin:

$$\dot{x} = f(x,t), \quad x \in \mathbb{R}^n, t \in \mathbb{R}_+ \tag{8}$$

Stability definitions—The origin is a stable equilibrium of the system (8) in the sense of Lyapunov for a given t_0, if for every $\epsilon > 0$ there exists a $\delta > 0$ such that

$$\|x(t_0)\| \leq \delta \implies \|x(t_0 + t)\| \leq \epsilon \quad \forall t \geq 0 \tag{9}$$

If the system is stable and there is a δ such that

$$\|x(t_0)\| \leq \delta \implies x(t_0 + t) \to 0 \text{ as } t \to \infty, \tag{10}$$

the system is considered asymptotically stable. The region of attraction is the set of all initial states from which the trajectories converge to the origin. The system is *globally asymptotically stable* when this condition holds for all δ. If these conditions hold for all $t_0 \in \mathbb{R}$, the system is uniformly (globally and/or asymptotically) stable.

Theorem 2.1 (Lyapunov direct method: time-invariant systems) Suppose that there exists a positive definite $\mathcal{C}^\infty$ function $V : \mathbb{R}^n \to \mathbb{R}$ outside the origin with $V(0) = \dot{V}(0) = 0$.

If $\dot{V}(x)$ is negative semidefinite outside the origin along solutions of the system in Eq. (8), it is called a *weak Lyapunov function* and it proves the (local) Lyapunov stability of the origin of the system.

If $\dot{V}(x)$ is strictly negative definite outside the origin, it is called a *(strict) Lyapunov function* and it proves the (local) asymptotic stability of the origin of the system. If the

function is also radially unbounded, the stability property holds globally.

We note that these results are still valid in the case of a non-differentiable continuous function $V(x)$ as long as it strictly decreases at nonzero function values or is nonincreasing.

A weak Lyapunov function can still prove asymptotic stability under the invariance principle. To define this, we must first establish the definition of an *invariant set* as any set M for which $x(t_0) \in M$ means that $x(t) \in M \; \forall \, t \in \mathbb{R}$, and a positively invariant set if it means that $x(t_0 + T) \in M \; \forall \, T \in \mathbb{R}_+$.

Theorem 2.2 (LaSalle invariance principle) Suppose that there exists a weak Lyapunov function in the domain Ω. Let M be the largest invariant set contained in the set $E = \{\dot{V}(x) = 0\}$. Then every solution starting in Ω asymptotically approaches M.

Two useful corollaries to the invariance principle (Barbashin and Krasovskii's theorems) state that, if no solution other than the origin will stay in the set E, then the origin will be (globally) asymptotically stable.

For time-varying systems, Theorem 2.1 can still apply with a time-varying Lyapunov function $V(x, t)$. To prove uniform (asymptotic) stability, the additional condition that $V(x, t)$ be decrescent ($V(0, t) = 0$ and $V(x, t) \leq V(x) \; \forall t \geq 0$ is needed. The equivalent to the invariance principles for time-varying systems is Barbalat's lemma.

Lemma 2.3 (Barbalat's Lyapunov-like lemma) If a scalar function $V(x, t)$ satisfies the following conditions

- $V(x, t)$ is lower bounded
- $\dot{V}(x, t)$ is negative semi-definite
- $\dot{V}(x, t)$ is uniformly continuous in time

then $\dot{V}(x, t) \to 0$ as $t \to \infty$, and V approaches a finite limiting value $V_\infty \leq V(x(0), 0)$.

A sufficient condition for a differentiable function to be uniformly continuous is that its derivative be bounded.

Another useful version of Barbalat's lemma is the one presented in [18], as follows:

Lemma 2.4 (Barbalat's Lyapunov-like lemma extension) Consider a smooth nonlinear time-varying system $\dot{x} = f(x, t)$. Assume a positive definite Lyapunov function $V(x) > 0 \, \forall \, x \neq 0$, the gradient of which is zero at the origin and $\neq 0$ everywhere else. The states will converge to one of the system's equilibria if the following conditions are satisfied:

1. $\dot{V}$ is negative semi-definite,

2. $\dot{V}$ is uniformly continuous,

3. The level sets S of V do not contain any integral curves $x(t)$ of the flow map $f(x, t)$ other than the constant ones.

If the origin is the only one, it is globally asymptotically stable.

To prove positive invariance of a set, Nagumo's theorem is typically used [19].

3. SPIN-STABILIZED POINTING CONTROLLER

The controller follows Algorithm 1, where we define the following:

- $s(t)$: Target direction in the body frame at time t
- $b(t)$: Magnetic field in the body frame at time t
- $\omega(t)$: Angular velocity of the body frame with respect to the inertial frame expressed in the body frame at time t
- $\overline{h}$: Target angular momentum in the body frame
- J: Inertia matrix
- a: Target major/minor axis of inertia direction
- tol_{SS}: Tolerance for spin-stabilizing control
- tol_{P}: Tolerance for sun-pointing control
- $\hat{b}$: Skew symmetric matrix corresponding to the cross product with the magnetic field
- $\mu_{\max}$: Maximum magnetic dipole moment
- μ: Commanded total magnetic dipole moment in the body frame

In addition, we define a generic scalar smoothing function class $\alpha(r) : [0, \infty) \to [0, 1]$ if:

1. $\lim_{r \to 0} \alpha(r) = 0$,
2. α is strictly increasing $\left(\dfrac{d\alpha}{dr}(r) > 0 \right)$,
3. $\lim_{r \to \infty} \alpha(r) = 1$
4. $\alpha \in C^p, p \geq 1$

Algorithm 1 Lyapunov-based Sun-pointing controller

Input $: s, b, \omega$
Output $: u$

$h = J\omega$
if $\left\| a - \left(h / \left\| \overline{h} \right\| \right) \right\| > \text{tol}_{\text{SS}}$ **then**
  $\mu_b' = \hat{b} \left(\overline{h} - h \right)$
  $\mu = \mu_b = \mu_{max} g_b(\mu_b')$
else if $\left\| s - \left(h / \left\| \overline{h} \right\| \right) \right\| > \text{tol}_{\text{P}}$ **then**
  $\mu_i' = \hat{b} \left(s \left\| \overline{h} \right\| - h \right)$
  $\mu = \mu_i = \mu_{max} g_i(\mu_i')$
else
  $\mu = \mu_0 = [0 \quad 0 \quad 0]^T$
end if

return μ

This algorithm can also be expressed by the logic diagram shown in Fig. 2.

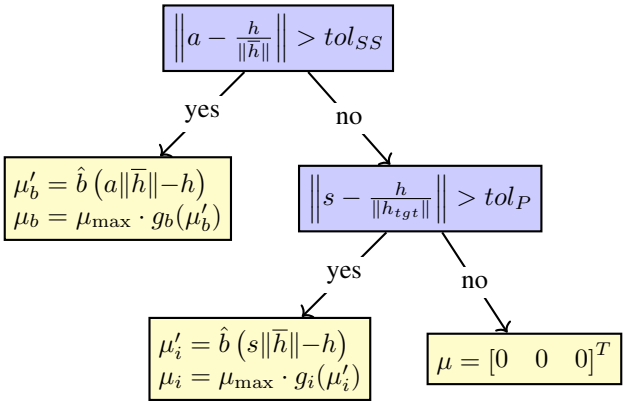

Figure 2. Logic diagram of the controller.

The goal of this algorithm is to drive the system described in (7) to a forward invariant set of states that respects the spin-stabilized and sun-pointing conditions, and is Lyapunov stable with respect to the equilibrium $h_0 = \overline{h}, s_0 = a$.

In this paper, we differentiate between smooth and non-smooth versions of the algorithm through the functions g and the smoothing functions α that can be used to make the control law differentiable when $\|\mu'\| = 0$. For the non-smooth case, it is sufficient to consider $g(x) = x/\|x\|$. For the smooth case, we consider:

$$g(\mu) \equiv \tilde{\mu} = \begin{cases} \alpha(\|\mu\|)\frac{\mu}{\|\mu\|}, & \|\mu\| \neq 0 \\ 0, & \|\mu\| = 0 \end{cases}, \tag{11}$$

with $\alpha(x) = \tanh(kx)$, with $k \in \mathbb{R}^+$ some positive scalar control gain.

The version of the algorithm in this paper also differs from the one described in [13] in that the pointing condition and controller are defined based on $\|s - h/\|\overline{h}\|\|$ instead of $\|s - h/\|\overline{h}\|\|$. The use of $\|h\|$ defines a conical region for the angular momentum to meet the pointing condition, such that it is met when the angular momentum and target direction are within a given angle. In practice, since the pointing condition and controller are only used when the spin-stabilized condition is met, the difference between the values of $\|h\|$ and $\|\overline{h}\|$ will be limited by the tolerance tol_{SS} and should be relatively small. In this work, we focus on the version of the algorithm that uses $\|\overline{h}\|$ for the sake of simplicity, and leave the version described in [13] for future work.

Stability Analysis

To study the stability of the system under the proposed control law, we define the two following candidate Lyapunov functions:

$$\begin{cases} V_i(x) = \frac{1}{2}(h - \|\overline{h}\|s)^T(h - \|\overline{h}\|s) \\ V_b(x) = \frac{1}{2}(h - \overline{h})^T(h - \overline{h}) \end{cases} \tag{12}$$

A set of auxiliary variables x^* are defined so that the equilibrium is shifted to the origin ($x_0^* = 0$):

$$x^* = \begin{bmatrix} h^* \\ s^* \end{bmatrix} = \begin{bmatrix} h - \overline{h} \\ h - s\|\overline{h}\| \end{bmatrix} \tag{13}$$

The dynamics expressed as a function of the auxiliary variables are:

$$\underbrace{\begin{bmatrix} \dot{h}^* \\ \dot{s}^* \end{bmatrix}}_{\dot{x}^*} = \begin{bmatrix} \dot{h} \\ \dot{h} - \dot{s}\|\overline{h}\| \end{bmatrix} = \begin{bmatrix} -\omega \times h + \mu \times b(t) \\ -\omega \times s^* + \mu \times b(t) \end{bmatrix}$$

$$\dot{x}^* = \underbrace{\begin{bmatrix} (h^* + \overline{h}) \times \left(J^{-1}(h^* + \overline{h})\right) + \mu \times b(t) \\ s^* \times (J^{-1}(h^* + \overline{h})) + \mu \times b(t) \end{bmatrix}}_{f(x^*, \mu, t)} \tag{14}$$

The candidate Lyapunov functions can be rewritten as:

$$\begin{cases} V_i(x^*) = \frac{1}{2}(s^*)^T s^* \\ V_b(x^*) = \frac{1}{2}(h^*)^T h^* \end{cases} \tag{15}$$

Each of these functions meet the criteria for a candidate Lyapunov function with respect to their respective partial equilibria: $V_i(s_0^* = 0) = 0$ and $V_i(s^*) > 0 \ \forall \|s^*\| \neq 0$, $V_b(h_0^* = 0) = 0$ and $V_b(h^*) > 0 \ \forall \|h^*\| \neq 0$. Additionally, the functions are radially unbounded. Neither of these functions individually meet the criteria for the full equilibrium $x^* = 0$, although a candidate Lyapunov function for it can be built from the two. The switching conditions of the algorithm can be defined as a function of these auxiliary variables and/or the Lyapunov functions:

$$\left\|a - \frac{h}{\|\overline{h}\|}\right\| > \text{tol}_{\text{SS}} \equiv V_b > \underbrace{\frac{\left(\|\overline{h}\|\text{tol}_{\text{SS}}\right)^2}{2}}_{\overline{V}_b} \equiv \|h^*\| > \underbrace{\|\overline{h}\|\text{tol}_{\text{SS}}}_{\overline{h}^*} \tag{16}$$

$$\left\|s - \frac{h}{\|\overline{h}\|}\right\| > \text{tol}_{\text{P}} \equiv V_i > \underbrace{\frac{\left(\|\overline{h}\|\text{tol}_{\text{P}}\right)^2}{2}}_{\overline{V}_i} \equiv \|s^*\| > \underbrace{\|\overline{h}\|\text{tol}_{\text{P}}}_{\overline{s}^*} \tag{17}$$

The behavior of the system (7) under the described control law can be seen as a switched system [17], with three operating regions Ω_b, Ω_i and Ω_0 described by the application of the control laws μ_b, μ_i and μ_0, respectively. These operating regions are separated by three switching surfaces $\mathcal{S}_{ib}$, $\mathcal{S}_{i0}$ and $\mathcal{S}_{b0}$. The switching surface $\mathcal{S}_{ib}$ is defined by the spin-stabilized condition when the pointing condition is not met. $\mathcal{S}_{b0}$ is defined by the spin-stabilized condition when the pointing condition is met (crossing between Ω_b and Ω_0) and $\mathcal{S}_{i0}$ defines the pointing condition while the spin-stabilized condition is met (crossing between Ω_i and Ω_0).

The domain of the operating regions and the switching surfaces is defined in (18) and (19), respectively. They are also notionally represented in Fig. 3.

$$\begin{cases} \Omega_i = \left\{ x^* \middle| \left(V_b < \overline{V}_b\right) \cap \left(V_i > \overline{V}_i\right) \right\} \\ \Omega_b = \left\{ x^* \middle| V_b > \overline{V}_b \right\} \\ \Omega_0 = \left\{ x^* \middle| \left(V_b < \overline{V}_b\right) \cap \left(V_i < \overline{V}_i\right) \right\} \end{cases} \tag{18}$$

$$\begin{cases} \mathcal{S}_{ib} = \left\{ x^* \middle| \left(V_b = \overline{V}_b\right) \wedge \left(V_i > \overline{V}_i\right) \right\} \\ \mathcal{S}_{i0} = \left\{ x^* \middle| \left(V_b < \overline{V}_b\right) \wedge \left(V_i = \overline{V}_i\right) \right\} \\ \mathcal{S}_{b0} = \left\{ x^* \middle| \left(V_b = \overline{V}_b\right) \wedge \left(V_i < \overline{V}_i\right) \right\} \end{cases} \tag{19}$$

Within these regions, the control laws can also be rewritten as:

$$\begin{cases} \mu_b' = \hat{b}h^*, \quad \mu_i' = \hat{b}s^* \\ \mu_b = -\mu_{\max} \dfrac{\mu_b'}{\|\mu_b'\|} \alpha_b = -\mu_{\max} \hat{\mu}_b \alpha_b = -\mu_{\max} \tilde{\mu}_b \\ \mu_i = -\mu_{\max} \dfrac{\mu_i'}{\|\mu_i'\|} \alpha_i = -\mu_{\max} \hat{\mu}_i \alpha_i = -\mu_{\max} \tilde{\mu}_i \end{cases} \tag{20}$$

As a note, in the non-smooth case ($\alpha = 1$), these control laws each serve as the solution to the local/instantaneous minimization of the time derivative of the candidate Lyapunov functions $\dot{V}_b$ and $\dot{V}_i$ for the axisymmetric case:

$$\begin{aligned} \min_{\mu} \quad & \dot{V}(\mu) \\ \text{s.t.} \quad & \|\mu\|_2^2 \leq \mu_{\max}^2 \end{aligned}$$

The stability of the system with respect to the equilibria $h^* = 0$ and $s^* = 0$ is studied through the candidate Lyapunov functions V_i and V_b in the different operating regions and switching surfaces in Appendix A. The range of the derivatives of the two Lyapunov functions in the different operating regions and sliding mode is summarized in Table 1 and in the XY plot in Figure 3 for the axisymmetric case.

Table 1. Set of possible values of V_i, V_b, $\dot{V}_i$ and $\dot{V}_b$ in the different operating regions and the switching surface $\mathcal{S}_{ib}$ in the axisymmetric case.

	Ω_i	Ω_b	Ω_0	$\mathcal{S}_{ib}$
V_i	$(\overline{V}_i, \infty)$	$\mathbb{R}$	$[0, \overline{V}_i)$	$(\overline{V}_i, \infty)$
V_b	$[0, \overline{V}_b)$	$(\overline{V}_b, \infty)$	$[0, \overline{V}_b)$	$\{\overline{V}_b\}$
$\dot{V}_i$	$\mathbb{R}_{\leq 0}$	$\mathbb{R}$	$\{0\}$	$\mathbb{R}_{\leq 0}$
$\dot{V}_b$	$\mathbb{R}$	$\mathbb{R}_{\leq 0}$	$\{0\}$	$\mathbb{R}_{\leq 0}$

If we consider the smooth version of μ_b, the proof of uniform asymptotic stability to the equilibrium $h^* = 0$ under this control law in Ω_b is provided in Appendix A.

Let the union of the switching surfaces $\mathcal{S}_b := \mathcal{S}_{ib} \cup \mathcal{S}_{b0} := \{x^* : V_b = \overline{V}_b\}$. Because for $x^* \in \Omega_b$, as a consequence of $h^* = 0$ being uniformly asymptotically stable, $\|h^*\| \to 0$ and $V_b \to 0$. Therefore, for any $\overline{V}_b > 0$ and $t_0 \in \mathbb{R}$ such that $V_b(x^*(t_0), t_0) > \overline{V}_b$, there exists a finite time T such that $V_b(x^*(t), t) < \overline{V}_b$, $\forall t \geq t_0 + T$. Hence, the system will reach the surface $\mathcal{S}_b$.

The union of the operating regions $\Omega_{i0} := \Omega_i \cup \Omega_0$ is a sublevel set of the Lyapunov function V_b, and as established in the Appendix A, $\nabla V_b \cdot F_b(x^*) = 2h^* \cdot F_b(x^*) \leq 0 \; \forall \mathcal{S}_b$, with $\dot{x}^* \in F_b(x^*)$ the differential inclusion on the boundary/ level set of V_b $\mathcal{S}_b := \mathcal{S}_{b0} \cup \mathcal{S}_{ib}$. According to the Nagumo Theorem [20], the set Ω_{i0} will then be positively invariant, since the flow map on the bonudary belongs to the tangent cone. As such, once the system reaches Ω_{i0} from Ω_b, it stays in Ω_{i0} indefinitely.

For the smooth case, if we assume that the equilibrium $s^* = 0$ is uniformly asymptotically stable in the sense of Lyapunov for $x^* \in \Omega_i \cup \mathcal{S}_{ib}$, that V_i is a (weak) Lyapunov function for this equilibrium, and that $\mathcal{S}_{i0}$ is a level set of V_i, then it can be proven that any trajectory starting/entering in $\Omega_i \cup \mathcal{S}_{ib}$ will reach $\mathcal{S}_{i0}$ in finite time. This conclusion is currently limited by the existence of a local equilibrium in $\mathcal{S}_{ib}$, as described in Appendix A. If the equilibrium is unstable, it will not affect the convergence of the system to the target $s^* = 0$ for $x^* \in \Omega_i \cup \mathcal{S}_{ib}$ outside the local equilibrium itself. The study of this equilibrium is left to future work.

The target set for the controller is the torque-free operating region Ω_0. With $\dot{V}_i(x^*, t) = \dot{V}_b(x^*, t) = 0 \; \forall x^* \in \Omega_0$, uniform Lyapunov stability with respect to the equilibrium $x^* = 0$ can be proved with a valid joint Lyapunov function (the max or sum of the V_b and V_i, for example) in the axisymmetric case.

Under the Nagumo Theorem [20], a set is positively invariant if the flow map on the boundary of the set belongs to its tangent cone. The solution to the flow map on the boundary $\mathcal{S}_{b0}$ in the sense of Filippov will be the convex hull of the flow map on both ends, for which $\dot{V}_b \leq 0$. Similarly, the set of solutions for the flow map on $\mathcal{S}_{i0}$ will always meet the condition $\dot{V}_i \leq 0$. Since these flow maps on the boundary will point inwardly to the set Ω_0, the set Ω_0 is positively invariant, and any trajectory entering the set will stay there, with $|h^*| \leq \overline{h}^*$ and $|s^*| \leq \overline{s}^*$.

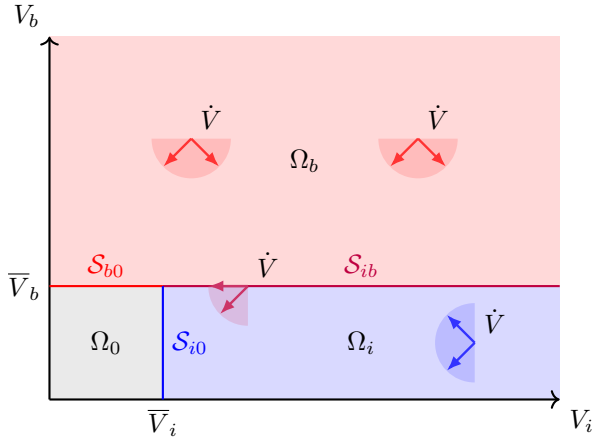

Figure 3. Notional representation of the operating regions and switching surfaces of the controlled system with possible flow maps in the operating regions.

4. Numerical Simulation Experiments

This section is dedicated to the numerical results and validation of the Lyapunov-based controller. It is split into two subsections: firstly, results are presented for the axisymmetric case to validate the conclusions of the proof of convergence

in Section 3. Secondly, numerical results are extended to the tri-inertial case and the PY4 mission. All the code used to produce these numerical simulations is available in our open-source implementation on Github[2].

Axisymmetric case

To validate the conclusions of the proof of convergence, simulations are run restricted to the axisymmetric case in a high-inclination Sun-synchronous (SSO) orbit. Additionally, a noise-free case study is singled out to exemplify the behaviors discussed in Section 3 and Appendix A.

A Monte Carlo simulation with 100 cases is run with the SSO orbital parameters described in Table 2. Assuming a diagonal inertia matrix with $J_{xx} = J_{yy} = J_\perp$ and $J_{zz} = J_\parallel$, we define the scenario for the pointing of the minor axis of a 2U CubeSat ($J_\perp$ =8.3 $\times$ 10^{-3} kgm^2 , $J_\parallel$ =3.3 $\times$ 10^{-3} kgm^2). The controller uses a smoothing function $\alpha_i = \tanh\left(k\|\mu_i'\|/\|\bar{h}\|\right)$ and $\alpha_b = \tanh\left(k\|\mu_b'\|/\|\bar{h}\|\right)$, with $k = 1e5$. We considered a gyro bias $\omega_b \sim \mathcal{N}\left(0, \sigma_{\omega_b}^2\right), \sigma_{\omega_b} = 0.1^\circ s^{-1}$ and gyro additive white gaussian noise (AWGN) with $\sigma_\omega = 0.007^\circ s^{-1}/\sqrt{Hz}$. The magnetometer and sun sensor errors are modeled as AWGN with $\sigma_b = 0.5\mu T/\sqrt{Hz}$ and $\sigma_s = 0.01/\sqrt{Hz}$, respectively. The sun sensor measurement is re-normalized after the error is added. The simulations were initialized with the satellite tumbling at an angular velocity ω_0 sampled from a normal distribution with standard deviation $10^\circ/s$ at an arbitrary attitude. The Sun vector was initialized as,

$$s_0 = \begin{bmatrix} 1 \\ 0 \\ 0 \end{bmatrix}, \tag{21}$$

with an uncertainty of 10% added in a random direction.

Figure 4 shows the percentiles and average of the normalized angular momentum error $\|h^*\|/\|\bar{h}\|$ and the angle between the angular momentum and target direction against the respective thresholds. All trajectories spin-stabilize within around half an hour and then align the angular momentum with the target within around an hour and a half. Once these conditions are reached, the target (sun) direction stays in the vicinity of the spin axis, as shown in the plot of the angle between the sun and the minor axis in Figure 5.

The Monte Carlo simulation results align with the expected behavior from the lyapunov stability analysis. Additionally, all trajectories converge to the final Lyapunov stable configuration within the prescribed tolerances ($\text{tol}_{\text{SS}} = 0.26$ and $\text{tol}_{\text{P}} = 0.15$, respectively). However, under the stability analysis, any trajectory entering the final Ω_0 region would stop converging to the origin once crossing the set boundary, whereas in the numerical simulations the error continues falling after entering the region as a consequence of the measurement noise.

A single simulation is run without any measurement noise. The values of the $\|h^*\|/\|\bar{h}\|$ and $\|s^*\|/\|\bar{h}\|$ over the simulation are plotted in Figure 6. Fig. 1 shows the trajectory of the angular momentum in the body frame of the single simulation, indicating what operating region/switching surface the system is in.

[2] https://github.com/RoboticExplorationLab/Sun_Pointing_Lyapunov

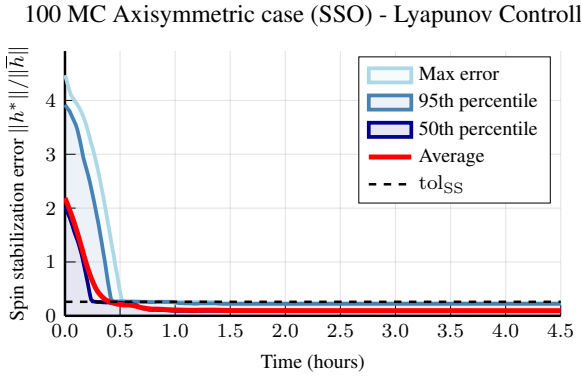

(a)Spin Stabilization error $\|h^*\|/\|\bar{h}\|$.

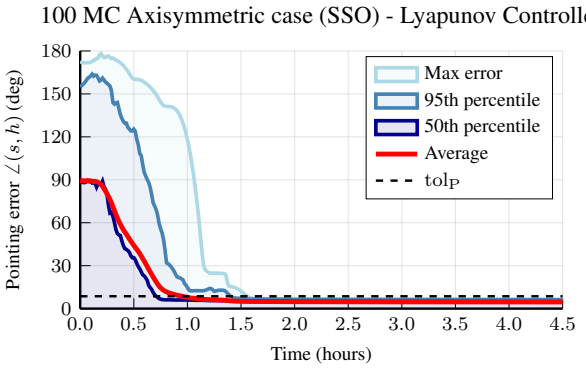

(b)Angle between the target direction s and the angular momentum h.

Figure 4. Time evolution of the spin stabilization and pointing error in 100 Monte Carlo runs. Notice how in every case the controller is able to bring both Spin Stabilization error and Sun-Pointing error to the tolerances.

General case

This section presents two simulation cases that demonstrate the performance of the controller extended to a tri-inertial condition. We consider a satellite in a high-inclination Sun-synchronous orbit, and an ISS-like low-inclination orbit.

Numerical analyses consider the PY4 mission [13]. These simulations were run in preparation for flight and subsequent comparison. We also did simulations to demonstrate performance at a different relevant LEO condition. Sun-synchronous numerical simulations were based on planned orbit parameters given by the launch provider and inertia matrix J calculated from CAD drawings of the satellite. A fourth-order Runge-Kutta (RK4) integrator [21] was used to run the simulations.

$$J = \begin{bmatrix} .0043 & -.0003 & 0.0 \\ -.0003 & .0049 & 0.0 \\ 0.0 & 0.0 & .0035 \end{bmatrix} \tag{22}$$

Measurement noise was again considered, as described for the axisymmetric case study. The initial angular velocity and sun vector conditions were also dispersed similarly. The desired angular momentum for flat-spin is the major axis of inertia, a:

$$a = \begin{bmatrix} -0.38268 \\ 0.92388 \\ 0 \end{bmatrix} \tag{23}$$

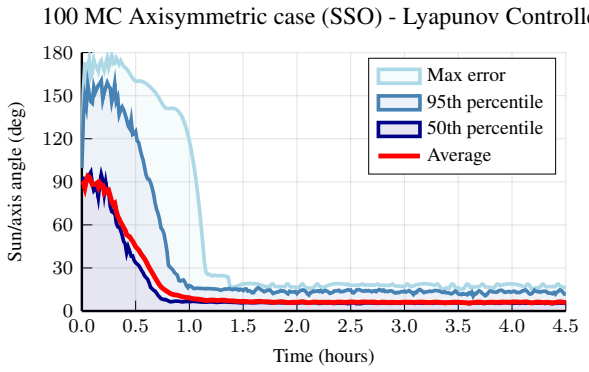

Figure 5. Angle between the (pointed) minor axis and the sun vector in the prolate 2U axisymmetric case. The controller is able to converge to the final region in all 100 runs within a few hours.

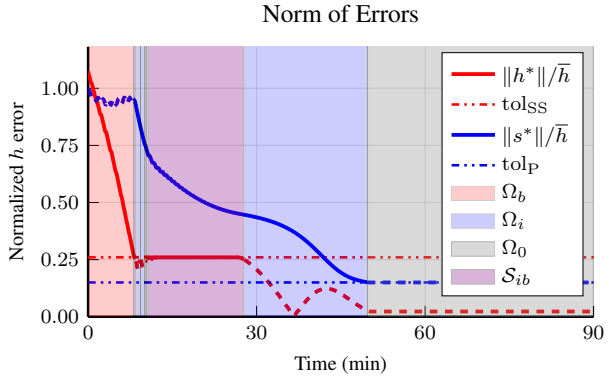

Figure 6. Time evolution of $\|h^*\|/\|\bar{h}\|$ and $\|s^*\|/\|\bar{h}\|$ for the 2U axisymmetric case, in the absence of measurement noise. These are compared with the thresholds for switching control laws. The background color describes the operating region Ω or switching surface $\mathcal{S}$ the system is in at a given time.

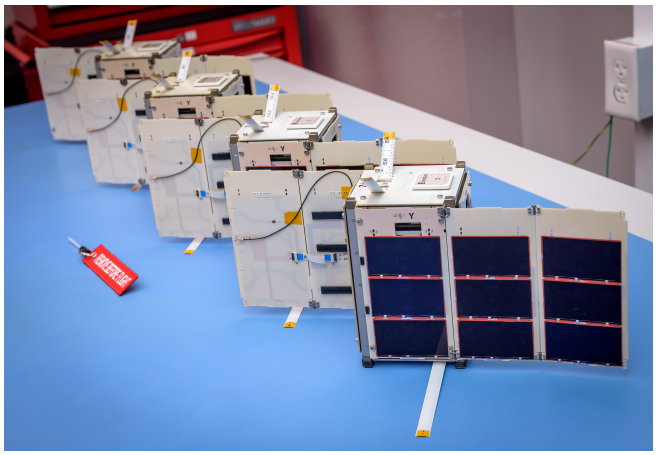

Figure 7. PY4 is a four-satellite demonstrator of range-based relative orbit determination and advanced GNC algorithms. The controller presented in this work is especially relevant to missions like PY4 as a low-compute safe mode that provides stability guarantees. The controller presented in this paper was successfully tested on orbit in two separate occasions, on PY4-A and PY4-B.

The Lyapunov control law adopted in these simulations is smooth, with the same smoothing function as the one described for the axisymmetric case.

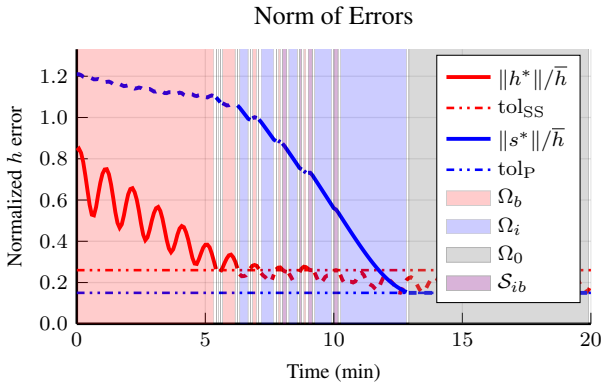

Figure 8. Time evolution of $\|h^*\|/\|\bar{h}\|$ and $\|s^*\|/\|\bar{h}\|$ for the triaxial case seen in PY4 during sun synchronous orbit, with no measurement noise or parameter dispersion. These are compared with the thresholds for switching control laws. The background color describes the operating region Ω or switching surface $\mathcal{S}$ the system is in at a given time.

A single simulation is run with no measurement noise or inertia uncertainty. The values of $\|h^*\|/\|\bar{h}\|$ and $\|s^*\|/\|\bar{h}\|$ over the simulation are plotted in Figure 8. These results exemplify how several of the conclusions from the stability analysis of the axisymmetric case do not apply to the tri-inertial case. As can be seen, the value of $\|h^*\|$ (and V_b by extension) does not decrease monotonically in Ω_b, the system can cross back into Ω_b after reaching Ω_{i0} and V_b is not necessarily constant at Ω_0. The target region is still reached, however.

We ran 100 Monte-Carlo (MC) simulations in each starting condition. Fig, 9 shows the angular momentum error with respect to the Sun vector in a Sun-synchronous orbit at 600 km altitude and an inclination of 95°.

Table 2. Monte-Carlo Initial Conditions

Satellite State	SSO	LEO
Altitude	600km	490km
Eccentricity	0	0
Inclination	95°	51.6°
RAAN	1°	1°
Arg. of Perigee	28°	28°
Mean Anomaly	190°	190°

Convergence to the desired angular momentum direction is achieved in all MC runs, with an average spin axis/sun-pointing error of 6.05°. We implemented a baseline controller that uses a linear combination of spin stabilization and spin-axis pointing, whose control law μ is [4]

$$\mu = \frac{\hat{b}}{\|b\|^2}\left(k_{ss}\left(\bar{h}-h\right)+k_p\left(s\|\bar{h}\|-h\right)\right) \qquad (24)$$

.

The gains for the baseline were set to $k_p = k_s = k\bar{b}^2/\|\bar{h}\|$, with k the gain used for the smoothing function of the

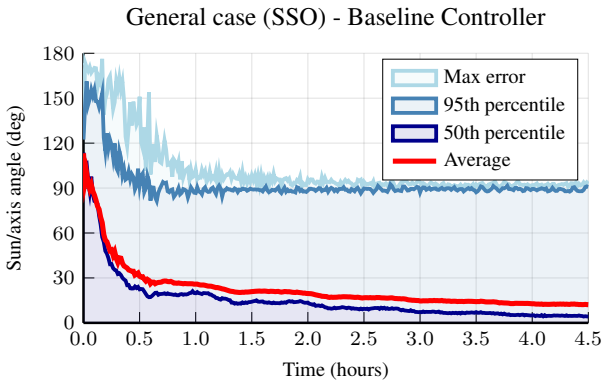

(a)Baseline

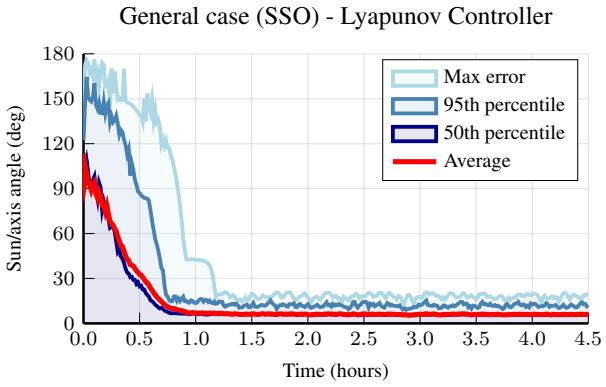

(b)Lyapunov-Based

Figure 9. A baseline controller Monte-Carlo experiment only succeeds in reaching the neighbourhood of the target equilibrium in 79% of the trajectories at SSO. The red line is the average of the error of all samples at a given time step. Notice that the trajectories above the 95th percentile do not converge to the target major axis spin. Our controller's Monte-Carlo experiment converges in all but one run to the target region and reaches an average accuracy of $6.05°$ of sun-pointing error at SSO. Notice that our controller presents little jittering, with all simulations reaching low steady-state error.

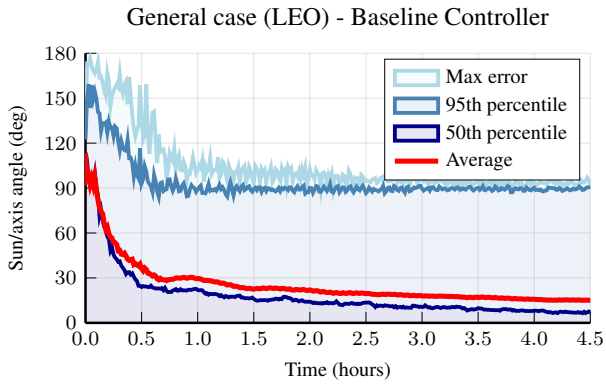

(a)Baseline

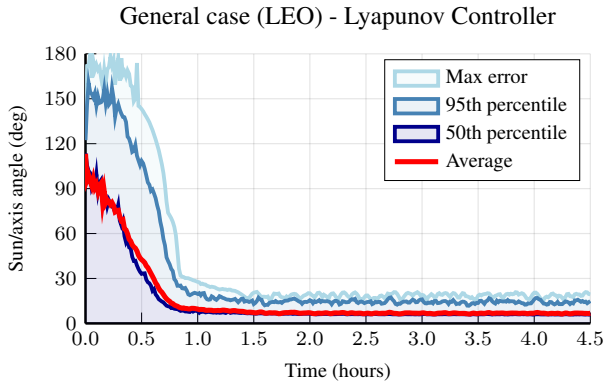

(b)Lyapunov-based

Figure 10. The baseline controller Monte-Carlo experiment reaches an average accuracy of $15.07°$ of sun-pointing error at LEO. The red line is the average of all samples at a given time stamp, while the blue curves show different percentiles. Once again, the worst cases of the baseline fail to achieve major axis spin. Our controller's Monte-Carlo experiment reaches an average accuracy of $6.77°$ of Sun-pointing error at LEO. It more consistently drives the system to the neighbourhood of the equilibrium under measurement noise and inertia uncertainty.

lyapunov controller and $\bar{b} = 2\text{e}{-5}$ a reference value in Tesla of roughly the order of magnitude of the geomagnetic field at an altitude of around 500km in LEO. The choice was made, based on the results of [4], to keep $k_p = k_s$. The norm of the magnetic dipole moment is upper bounded by $\mu_{\max}$, with saturation enforced by the correction $\mu' = \mu \cdot \min(1, \mu_{\max}/\|\mu\|)$. The reader is cautioned, however, that the value of the comparison between the controllers is limited by the tuning of the parameters of either approach.

Fig. 9 shows the result of the Monte-Carlo experiment at a sun-synchronous orbit. The baseline controller fails to converge to the target major axis spin in 9 of the 100 MC cases. In 12 simulations, it fails to align the angular momentum to within $\arcsin(\text{tol}_\text{p}) \approx 8.6°$ of the sun direction.

Fig. 10 shows the errors of the angular momentum vector with respect to the sun vector in a low-Earth Orbit (LEO) at 490km altitude and an inclination of $51.6°$. The lower orbital inclination is more challenging for the controllers due to less variation of the Earth's magnetic field. Convergence is achieved in all MC runs with our controller. The baseline controller fails in 10 simulations to spin-stabilize around the major axis and in 33 to sufficiently align the angular momentum with the sun direction.

In approximately 20% of trials in the SSO orbit and 43% of trials in the LEO orbit, the baseline controller fails to either achieve the desired angular rate or the alignment of the angular momentum to the sun within the defined tolerances. Table 3 shows the percentage of runs that reached the target Ω_0 region by the end of the simulation:

Table 3. The proposed controller is successful in nearly every run of the Monte Carlo campaign, with only one run missing the pointing threshold by a small margin, while the baseline only achieves a success rate of around 80% in SSO and 60% in LEO. .

	Baseline	Lyapunov switched
SSO	79%	99%
LEO	57%	100%

5. On-Orbit Validation

The PY4 [13] mission launched on March 4, 2024 aboard the Spacex Transporter 10 mission and demonstrated open-source, cost-effective inter-satellite ranging, high-data-rate mesh networking, and relative navigation. It served as a test bed for novel control techniques, such as the one presented in this work. Fig. 7 shows the the four satellites that flew in the PY4 mission.

All four satellites deployed and accomplished baseline mission requirements. The satellites were deployed at 515 km altitude at a high-inclination sun-synchronous orbit. The target major axis was

$$a_{tgt} = \begin{bmatrix} -0.2957 \\ 0.954 \\ 0.0438 \end{bmatrix} \tag{25}$$

Every plot shown is refactored to show the data relative to the principal axes. In this case, we set a_{tgt} as +Z. The transformations were

$$\omega_p = V^T \omega, \tag{26}$$

where ω_p is the angular velocities in each principal axis, V is a matrix with the three principal axes of inertia

$$V = \begin{bmatrix} 0.0 & 0.92388 & -0.382683 \\ 0.0 & 0.382683 & 0.92388 \\ 1.0 & 0.0 & 0.0 \end{bmatrix}, \tag{27}$$

and ω are the gyro measurements. The same transformation was applied to the Sun vector measurements:

$$s_p = V^T s, \tag{28}$$

where s_p are the Sun vector measurements expressed in each principal axis and s the measurements of the Sun vector in body frame.

Figs. 11 and 12 show the time series of sun sensor and gyro data from PY4-B collected over periods when our controller was activated, respectively. The non-smooth version of the controller implemented on the mission is described in [13]. The controllers were activated for two periods of around 20 minutes over the course of two days due to operational constraints (energy consumption and ground-station coverage). Each discontinuity in the data shows a moment where the controller was deactivated concatenated directly into the next activation. The data in Figs. 11 and 12 show four different activations of the controller on a period between March 28th, 2024 and March 29th, 2024 concatenated in a single plot. The plots in Figure 13 show the computed angles between the spin axis and the angular momentum, and between the angular momentum and the sun vector.

First, the satellite does a spin-stabilization maneuver, spinning to $12^\circ/s$ close to the 20 minute mark. It then remains spinning at this rate until a second activation, when the satellite reaches sun-pointing at an average of 14.27° error between the angular momentum and the sun vector s over the last five minutes of running, as seen in s_z sitting close to -1 from that point onward. At that point, the satellite is in a stable major-axis spin at $12^\circ/s$ with some nutation, which we attribute to a combination of sensor and actuator misalignment and uncertainty in the true major axis of the spacecraft. This configuration is a stable equilibrium, which ensures the satellite will remain in a sun-pointing spin passively after reaching this condition.

6. Conclusions

We have presented a controller that can reliably spin stabilize a spacecraft and point its spin axis at the sun to ensure positive power generation. The controller's exclusive reliance on low-cost lightweight sensors and magnetorquer actuators, and its low computational requirements, make it ideal for use on small resource-constrained spacecraft or as a safe-mode controller on larger spacecraft. An analytical stability study of the controller's behavior was made, and significant progress was achieved towards a proof of asymptotic convergence to a forward invariant set close to the target equilibrium under a smooth implementation of the control law for the axisymmetric case. Additionally, numerical simulations were run for the general tri-inertial case with a smooth implementation. The controller demonstrated excellent performance in both Monte-Carlo simulations and on orbit during the PY4 mission. In future work, we hope to generalize the Lyapunov stability analysis to the tri-inertial and the non-smooth cases, as well as the techniques developed in this paper to more general pointing scenarios and also to use cases with both magnetorquers and one-or-more reaction wheel actuators. We hope this controller can provide a reliable and low-cost attitude stabilization method for a variety of future missions.

Appendices

A. Operating regions and Switching Surface Stability

Stability of Ω_0

We start by studying the stability of the equilibrium in Ω_0. To this end, we evaluate the derivative of the two candidate Lyapunov functions, starting with $\dot{V}_i$:

$$\begin{aligned} \dot{V}_i &= (s^*)^T \dot{s}^* \\ &\overset{x\in\Omega_0}{=} s^* \cdot (-\omega \times s^*) = 0 \\ \dot{V}_b &= (h^*)^T \dot{h}^* \\ &\overset{x\in\Omega_0}{=} (h - \overline{h}) \cdot (-\omega \times h) = -\overline{h} \cdot (-\omega \times h) \end{aligned}$$

Lyapunov stability with respect to the partial equilibrium

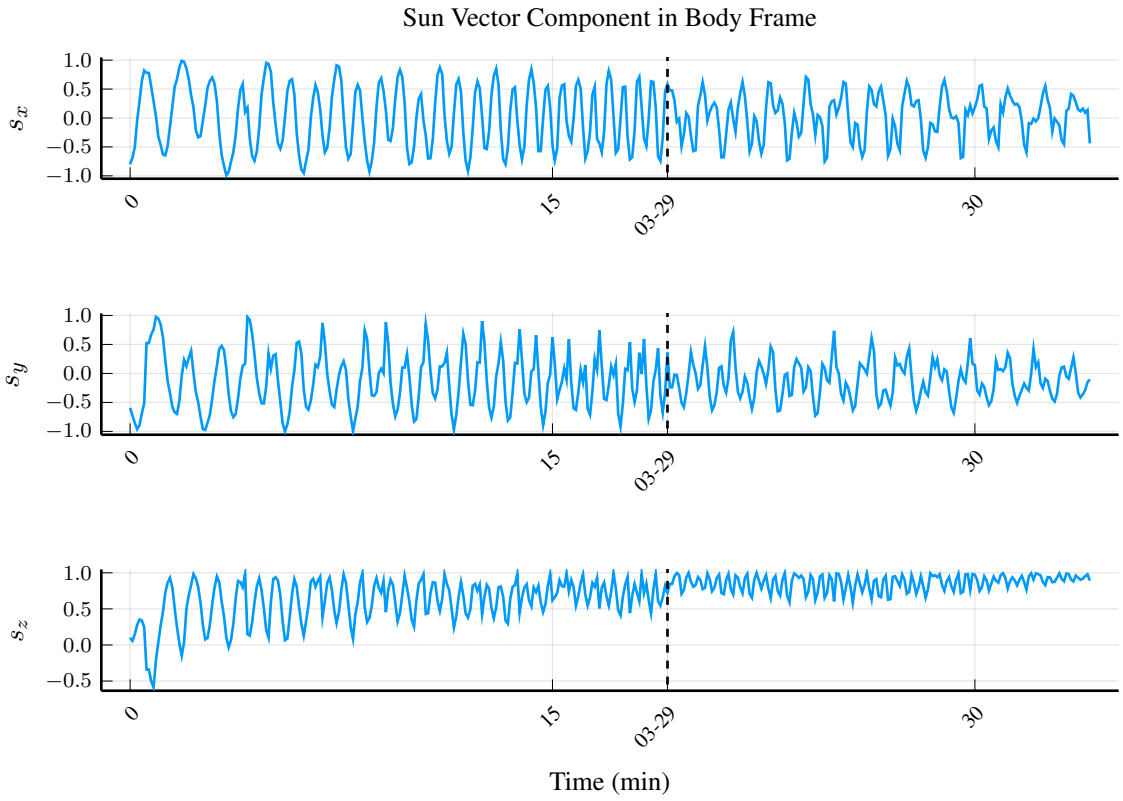

Figure 11. In two forty five-minute periods of running, PY4-A achieved Sun-pointing within 14.27^o of error on average for the last five minutes of this test run, giving flight heritage to the controller presented in this work. The Z axis shows steady pointing close to -1, proving that this axis is pointed to the Sun.

$s^* = 0$ is proven by the fact that $\dot{V}_i(s^*) = 0 \; \forall s^* \in \Omega_0$, following intuitively from the conservation of angular momentum in the absence of external torques. The partial equilibrium $h^* = 0$ in torque free-motion is known to be locally Lyapunov stable for major and minor axis spin equilibriums [22]. However, this choice of Lyapunov function is not adequate to the general tri-inertial case since nutation will lead to periodic oscillations in $\|h^*\|$ and V_b. For the sake of simplicity, we limit this analysis to the pointing of the major/minor axis in oblate/prolate axisymmetric bodies. We define this axis to be z in the body frame with moment of inertia $J_\parallel$, and $J_\perp$ around x and y. In this case, $\dot{V}_b = 0$, and Lyapunov stability can be verified with this candidate Lyapunov function for the equilibrium $h^* = 0$. Lyapunov stability with respect to the full equilibrium $x^* = 0$ can be proven with the combination of the two functions, with a joint Lyapunov function such as $V = V_i + V_b$.

As the set is defined by the states for which $V_b < \overline{V}_b$ and $V_i < \overline{V}_i$, and $\dot{V}_b(x^*) = \dot{V}_i(x^*) = 0 \; \forall x^* \in \Omega_0$. As such, this set is forward invariant, and any trajectory starting/entering Ω_0 will stay there.

Stability of Ω_b

The same process is applied to the operating region Ω_b:

$$
\begin{aligned}
\dot{V}_i &= (s^*)^T \dot{s}^* \\
&\overset{x \in \Omega_b}{=} (s^*)^T \left(-b(t) \times (-\mu_{\max} \tilde{\mu}_b)\right) \\
&= -\mu_{\max} (s^*)^T \hat{b}(t)^T \tilde{\mu}_b = -\mu_{\max} (\mu_i')^T \tilde{\mu}_b \\
\dot{V}_b &= (h^*)^T \dot{h}^* \\
&\overset{x \in \Omega_b}{=} -\mu_{\max} (h^*)^T \hat{b}(t)^T \tilde{\mu}_b \\
&= -\mu_{\max} \|\mu_b'\| \alpha_b \leq 0
\end{aligned}
$$

From the above, we conclude that the candidate Lyapunov function V_i will not be nonincreasing, since the inner product $(b(t) \times h^*) \cdot (b(t) \times s^*)$ can be negative and $\dot{V}_i$ positive. On the other hand, $\dot{V}_b \leq 0$, with $\dot{V}_b(x^*) = 0 \forall \|b(t) \times h^*\| = 0$. Because the function can have a null derivative outside the equilibrium, proving asymptotic Lyapunov stability requires some additional consideration. We designate the set $\mathcal{S}_{Eb} = \{x^* \in \Omega_b \; : \; b(t) \times h^* = 0, h^* \neq 0\}$. Lemma 2.4 [18] states that, if in addition to the established assumptions, $\dot{V}$ is uniformly continuous and if the only equilibrium set of $\dot{V} = 0$ is the origin, then the origin is globally asymptotically stable. For the smooth version of the algorithm, $\dot{V}_b$ is uniformly continuous. Thus, to prove uniformly asymptotic convergence to $h^* = 0$ under the μ_b control law for this system, we need to prove that no other equilibrium exists within $\mathcal{S}_{Eb}$.

For the smooth control law, $\mu = 0$ within $\mathcal{S}_{Eb}$. Being in

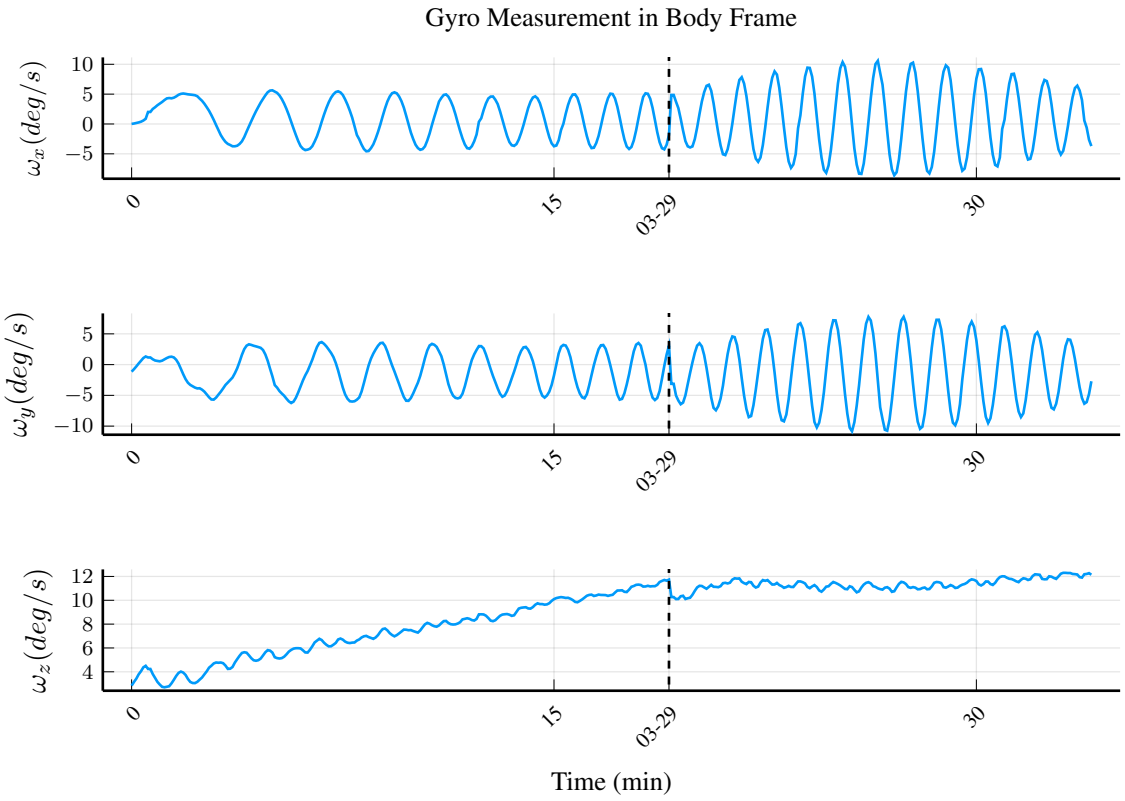

Figure 12. A trajectory of PY4's angular velocity displays an initial tumbling condition close to the x and y axes, with the spin-axis angle converging to the z direction at around $12^\circ/s$. The jitter at steady-state is due to nutation.

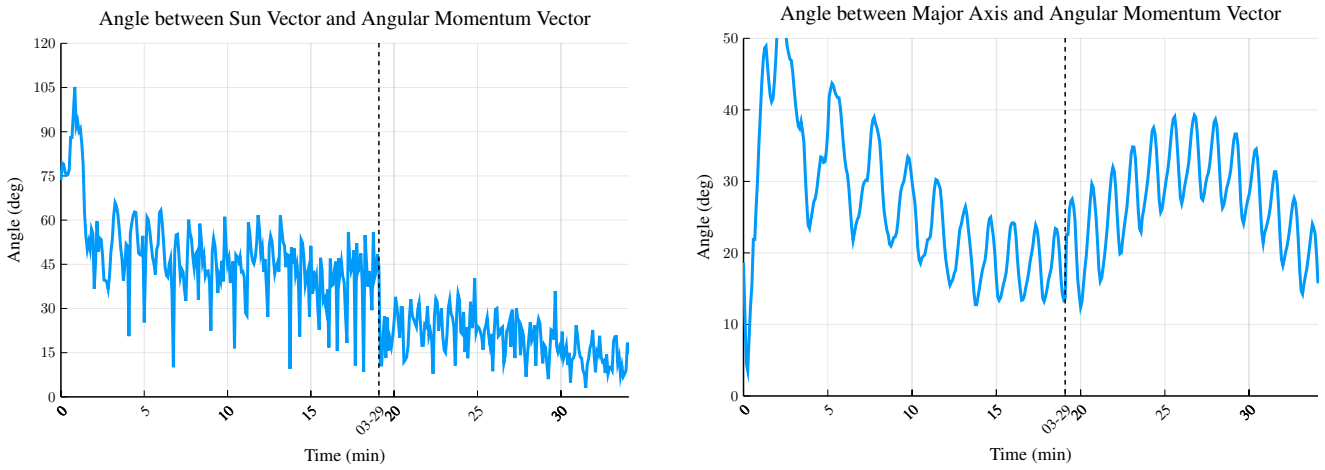

(a)Angle between target spin axis and angular momentum.

(b)Angle between the angular momentum and the sun direction.

Figure 13. Angles between the spin axis and the angular momentum and between the angular momentum and the sun direction from the PY4 mission. The Sun Vector and the Angular Momentum are on average 14.27° from each other in the last five minutes the controller was run. Notice there is nutation happening which pushes the major axis slightly away from the angular momentum direction.

$\mathcal{S}_{Eb}$ means that the angular momentum is parallel to $b(t)$, and without any control input this would have to hold in time, naturally. However, it has been shown in [18] and [23] that the angular momentum/angular velocity does not track the magnetic field in those conditions. As such, the equilibrium $h^* = 0$ will be uniformly asymptotically stable in Ω_b for the smooth control law.

Being in $\mathcal{S}_{Eb}$ means that the angular momentum is parallel to $b(t)$, and without any control input this would have to hold in time, naturally. However, it has been shown in [18] and [23] that the angular momentum/angular velocity does not track

the magnetic field in those conditions.

Stability of Ω_i

We now analyze the system under μ_i:

$$\begin{aligned}\dot{V}_i &= (s^*)^T \dot{s}^* \\ &\overset{x\in\Omega_i}{=} (s^*)^T \left(-b(t) \times \mu_{\max}\tilde{\mu}_i\right) \\ &= -\mu_{\max}\|\mu_i'\|\alpha_i \\ \dot{V}_b &= (h^*)^T \dot{h}^* \\ &\overset{x\in\Omega_i}{=} -\mu_{\max}(h^*)^T \hat{b}(t)^T \tilde{\mu}_i \\ &= -\mu_{\max}(\mu_b')^T \tilde{\mu}_i\end{aligned}$$

We see that $\dot{V}_i(x^*) \leq 0 \; \forall x^* \in \Omega_i$, with $\dot{V}_i(x^*) = 0$ when $\|b(t) \times s^*\| = 0$, for which the controller μ_i is not defined and the flow map f_i has a discontinuity in the non-smooth case. $\dot{V}_b$ will not be non-increasing, although by definition of the switching conditions $V_b < \overline{V}_b \forall x^* \in \Omega_i$. The equilibrium $s^* = 0$ is outside Ω_i, but the set $\mathcal{S}_{Ei} = \{x^* \in \Omega_i : \|b(t) \times s^*\| = 0, s^* \neq 0\}$ can still pose a challenge to the controller for achieving asymptotic stability to $s^* = 0$.

Similarly to the case with Ω_b, if a smooth iteration of μ_i is used, the control law in $\mathcal{S}_{Ei}$ will be $\mu_i = 0$. Under torque-free motion, it is trivial to show that s^* will not track the direction of the magnetic field b in the general case: with s^* composed of the sun direction and angular momentum, both constant in the inertial frame in the absence of external torques, under the assumption of persistence of excitation (constantly rotating b), then the set $\mathcal{S}_{Ei}$ will not hold local equilibriums. With $\dot{V}_i$ uniformly continuous, the equilibrium s^* can be said to be uniformly asymptotically stable under the smooth control law μ_i.

To study the behavior of the system at the switching surfaces, it's useful to define the vectors normal to these surfaces:

$$\begin{cases} n_{ib} = n_{b0} = \nabla(V_b - \overline{V}_b) = \nabla V_b = \begin{bmatrix} h^* \\ 0 \end{bmatrix} \\ n_{i0} = \nabla(V_i - \overline{V}_i) = \nabla V_i = \begin{bmatrix} 0 \\ s^* \end{bmatrix} \end{cases} \tag{29}$$

We can determine whether trajectories in an operation region will flow to or from the switching surface based on the value of $n^T f$ at the surface, which will coincide with $\nabla V f = \dot{V}$. The set of admissible solutions in the switching surface in the sense of Filippov is the convex hull of the flow map on either side of the surface [17]. Based on the found relations for the time derivatives of the two Lyapunov functions and the switching conditions in the different operating regions, it can be concluded that:

- Since $\dot{V} = 0 \; \forall x^* \in \Omega_0$ and Ω_0 is a sublevel set of the Lyapunov functions, Ω_0 is positively invariant and no trajectory will cross the switching surfaces $\mathcal{S}_{i0}$ and $\mathcal{S}_{b0}$ to Ω_b or Ω_i;
- Trajectories in Ω_b and Ω_i can cross $\mathcal{S}_{b0}$ and $\mathcal{S}_{i0}$ respectively into Ω_0;
- Trajectories in Ω_b can flow into but not from S_{ib}, while states in Ω_i can flow to and from $\mathcal{S}_{ib}$. This means that both crossings from Ω_b to Ω_i and sliding modes can occur.

Sliding mode on $\mathcal{S}_{ib}$

The solution in the sense of Filippov to the state flow map on $\mathcal{S}_{ib}$ whenever the state velocities in Ω_i and Ω_b flow against the surface will be the differential inclusion:

$$\dot{x}^* \in F_{ib}(x^*) \tag{30}$$

This differential inclusion will be defined by the convex hull of the flow maps of the neighboring operating regions in the vicinity of the switching surface:

$$F_{ib}(x^*) = \{\beta f_i(x^*) + (1-\beta) f_b(x^*) : \beta \in (0,1)\} \tag{31}$$

The exact solution for which the state trajectories describe a sliding mode is met when $n_{ib}^T f_{ib} = 0$:

$$\begin{aligned} &(h^*)^T(\beta(\dot{h}_i^*) + (1-\beta)(\dot{h}_b^*)) = 0 \\ \implies &(h^*)^T(-\omega \times h - b(t) \times (\beta\mu_i + (1-\beta)\mu_b)) = 0 \\ \implies &-(h^*)^T \left(\mu_{\max}\hat{b}(t)^T (\beta\tilde{\mu}_i + (1-\beta)\tilde{\mu}_b)\right) = 0 \\ \implies &\beta(\mu_b')^T\tilde{\mu}_i + (1-\beta)(\mu_b')^T\tilde{\mu}_b = 0 \\ \implies &\beta(\mu_b')^T\tilde{\mu}_i + (1-\beta)\|\mu_b'\|\alpha_b = 0 \implies \beta = \frac{\alpha_b}{\alpha_b - \hat{\mu}_b^T\tilde{\mu}_i} \end{aligned}$$

Then, the exact solution for the sliding mode is:

$$\begin{aligned} &\dot{x}^* = \beta f_i(x^*) + (1-\beta) f_b(x^*) \\ \implies &\begin{bmatrix} \dot{h}^* \\ \dot{s}^* \end{bmatrix} = \begin{bmatrix} -\omega \times h \\ -\omega \times s^* \end{bmatrix} + \begin{bmatrix} \hat{b}(t)^T \\ \hat{b}(t)^T \end{bmatrix} \underbrace{(\beta\mu_i + (1-\beta)\mu_b)}_{\mu_{ib}} \end{aligned}$$

$$\begin{aligned} \mu_{ib} &= \frac{\alpha_b}{\alpha_b - \hat{\mu}_b^T\tilde{\mu}_i}\left(-\mu_{\max}\tilde{\mu}_i\right) \\ &\quad + \left(1 - \frac{\alpha_b}{\alpha_b - \hat{\mu}_b^T\tilde{\mu}_i}\right)\left(-\mu_{\max}\tilde{\mu}_b\right) \\ \implies \mu_{ib} &= -\mu_{\max}\left(\frac{\tilde{\mu}_i - (\hat{\mu}_b^T\tilde{\mu}_i)\hat{\mu}_b}{1 - (\hat{\mu}_b^T\tilde{\mu}_i/\alpha_b)}\right) \end{aligned}$$

By definition, $V_b = \overline{V}_b$ in the sliding mode. To study the Lyapunov stability of the equilibrium $s^* = 0$ at $\mathcal{S}_{ib}$, V_i is once again used:

$$
\begin{aligned}
\dot{V}_i &= (s^*)^T \dot{s}^* \\
&= (s^*)^T \left(-\omega \times s^* + \hat{b}^T \mu_{ib}\right) \\
&= (s^*)^T \left(\hat{b}^T(-\mu_{\max}) \left(\frac{\tilde{\mu}_i - (\hat{\mu}_b^T \tilde{\mu}_i)\hat{\mu}_b}{1 - \hat{\mu}_b^T \tilde{\mu}_i/\alpha_b}\right)\right) \\
&= -\mu_{\max}(\hat{b}s^*)^T \left(\frac{\tilde{\mu}_i - (\hat{\mu}_b^T \tilde{\mu}_i)\hat{\mu}_b}{1 - (\hat{\mu}_b^T \tilde{\mu}_i/\alpha_b)}\right) \\
&= -\mu_{\max}(\mu_i')^T \left(\frac{\tilde{\mu}_i - (\hat{\mu}_b^T \tilde{\mu}_i)\hat{\mu}_b}{1 - (\hat{\mu}_b^T \tilde{\mu}_i/\alpha_b)}\right) \\
&= -\frac{\mu_{\max}\|\mu_i'\|\alpha_i}{1 - (\hat{\mu}_b^T \tilde{\mu}_i/\alpha_b)} \left(\hat{\mu}_i^T \hat{\mu}_i - (\hat{\mu}_i^T \hat{\mu}_b)(\hat{\mu}_b^T \hat{\mu}_i)\right) \\
&= -\frac{\mu_{\max}\|\mu_i'\|\alpha_i\alpha_b}{\alpha_b - (\hat{\mu}_b^T \hat{\mu}_i)\alpha_i} \left(1 - (\hat{\mu}_i^T \hat{\mu}_b)^2\right)
\end{aligned}
$$

In the smooth case, the negative semi-definiteness of $\dot{V}_i$ is dependent on the term $\alpha_b - (\hat{\mu}_b^T \hat{\mu}_i)\alpha_i$ being positive. With $\alpha_b, \alpha_i \in [0,1]$ and $\hat{\mu}_b^T \hat{\mu}_i \leq 0$ a necessary condition of the sliding mode in $\mathcal{S}_{ib}$, this term will be positive. In the specific non-smooth case ($\alpha = 1$), we get:

$$
\dot{V}_i = -\mu_{\max}\|\mu_i'\|\left(1 + (\hat{\mu}_i^T \hat{\mu}_b)\right) \leq 0 \tag{32}
$$

Because $\hat{\mu}_i$ and $\hat{\mu}_b$ are normalized vectors, $\|\hat{\mu}_i^T \hat{\mu}_b\| \leq 1$. Therefore, $\dot{V}_i \leq 0, \forall x^*$ in a sliding mode in $\mathcal{S}_{ib}$. Once again, proof of asymptotic convergence to $s^* = 0$ under this sliding mode requires the study of the set of states for which $\dot{V}_{ib} = 0$. This set is $\{x^* : (s^* = 0) \vee (b(t) \parallel s^*(t)) \vee (\hat{\mu}_i^T \hat{\mu}_b = -1)\}$.

We denote the subset of the switching surface $\mathcal{S}_{ib}$ for which the derivative of the Lyapunov functions is zero or the controller is not defined as $\mathcal{S}_{Eib}$ We split it into three subsets defining different edge cases $\mathcal{S}_{Eib} = \mathcal{S}_{Eib1} \cup \mathcal{S}_{Eib2} \cup \mathcal{S}_{Eib3}$:

1. $\mathcal{S}_{Eib1} = \{x^* \in \mathcal{S}_{ib} : \mu_i' = 0\}$
2. $\mathcal{S}_{Eib2} = \{x^* \in \mathcal{S}_{ib} : \mu_b' = 0\}$
3. $\mathcal{S}_{Eib3} = \{x^* \in \mathcal{S}_{ib} : 1 + \hat{\mu}_i^T \hat{\mu}_b = 0\} \setminus (\mathcal{S}_{Eib1} \cup \mathcal{S}_{Eib2})$

Each edge case is studied individually below. Following Lemma 2 from [18], we know that the system will be globally asymptotically Lyapunov stable if the isosurfaces S_E of $V(x)$ do not contain any integral curves $x(t)$ of the flow map other than the constant ones $x(t) = x_E$ at the equilibrium.

The configuration $\mathcal{S}_{Eib1}$ will occur at the intersection of the switching surfaces $\mathcal{S}_{ib}$ and the set $\mathcal{S}_{Ei} = \{x^* \in \Omega_i : \mu_i' = 0\}$, which was previously studied.

For the smooth case, $\mu_{ib} \in \{\beta\mu_b, \beta \in [0,1]\}$, such that the state trajectories will either stay in the surface if $\mu_{ib} = 0$ or enter Ω_i. For the case where it stays on the surface $\mathcal{S}_{ib}$, the same argument for why $\mathcal{S}_{Ei}$ will not hold any local equilibriums in the smooth case will apply to $\mathcal{S}_{Eib1}$. Similarly for $\mathcal{S}_{Eib2}$ for the smooth version, $\mu_{ib} \in \{\beta\mu_i, \beta \in [0,1]\}$. For $\mu_{ib} = 0$, the trajectory stays in $\mathcal{S}_{ib}$ and exits $\mathcal{S}_{Eib2}$ in the same way it would leave $\mathcal{S}_{Eb}$ in Ω_b.

The set $\mathcal{S}_{Eib3}$ is a subset of the sliding surface, rather than its intersection with other switching surfaces. It occurs when $1 + \hat{\mu}_i^T \hat{\mu}_b = 0$, for which the control on the sliding surface will be $\mu_{ib} = 0$. Expressing this set under the condition $\Phi(x^*) = \mu_i \times \mu_b = 0$ when $\mu_i^T \mu_b < 0$, and knowing that in this set there is a scalar $\beta = \|\mu_b\|/\|\mu_i\|$ such that the condition $\mu_b = -\beta\mu_i$ holds, we study whether it will hold any integral curves of the flow map f:

$$
\begin{aligned}
&\Phi = \mu_i \times \mu_b = 0 \quad \forall x^* \in \mathcal{S}_{Eib3} \\
&\dot{\Phi} = \dot{\mu}_i \times \mu_b + \mu_i \times \dot{\mu}_b \\
&\underbrace{=}_{\mu_b = -\beta\mu_i} \mu_i \times (\beta\dot{\mu}_i + \dot{\mu}_b) \\
&= \mu_i \times \left(\beta\dot{\mu_i'} + \dot{\mu_b'}\right) \\
&= -\mu_i \times \left(\beta(\dot{b} \times s^* + b \times \dot{s}^*) + \dot{b} \times h^* + b \times \dot{h}^*\right) \\
&= -\beta\mu_i \times \left(\left(-\omega \times b + R_b^i \dot{b}_i\right) \times s^* + b \times (-\omega \times s^*)\right) \\
&- \mu_i \times \left(\left(-\omega \times b + R_b^i \dot{b}_i\right) \times h^* + b \times \left(-\omega \times (h^* + \overline{h})\right)\right) \\
&= -\mu_i \times \left(\left(R_b^i \dot{b}_i\right) \times (\beta s^* + h^*)\right) \\
&+ \beta\mu_i \times (s^* \times (b \times \omega) + b \times (\omega \times s^*)) \\
&+ \mu_i \times \left(h^* \times (b \times \omega) + b \times (\omega \times (h^* + \overline{h}))\right) \\
&\underbrace{=}_{\text{Jacobi identity}} -\mu_i \times \left(\left(R_b^i \dot{b}_i\right) \times (\beta s^* + h^*)\right) \\
&- \mu_i \times \left(\beta\omega \times (s^* \times b) + \omega \times (h^* \times b) + b \times (\omega \times \overline{h})\right) \\
&= -\mu_i \times \left(\left(R_b^i \dot{b}_i\right) \times (\beta s^* + h^*)\right) \\
&- \mu_i \times \left(-\omega \times (\underbrace{\beta\mu_i + \mu_b}_{=0}) + b \times (\omega \times \overline{h})\right) \\
&\dot{\Phi} = -\mu_i \times \left(\left(R_b^i \dot{b}_i\right) \times (\beta s^* + h^*) + b \times (\omega \times \overline{h})\right)
\end{aligned}
$$

Under the assumption of persistence of excitation of the magnetic field ($R_b^i \dot{b}_i \neq 0 \forall t$, with b_i constantly changing orientation) and that $b \neq 0 \forall t$, for the above term to be zero, firstly $\omega \times \overline{h} = 0 \implies \omega \parallel \overline{h} \parallel h$, implying pure spin around the target axis. On the surface $\mathcal{S}_{ib}$, this leaves only two points where this condition is met, defined by the intersection between the target spin axis and the surface $\mathcal{S}_{ib}$. Secondly, $\beta s^* + h^* = 0$. This means s^* and h^* pointing in opposing directions, with the angular momentum h in the line between $s\|\overline{h}\|$ and $\overline{h}$. Since these two vectors have the same magnitude, the only point where this may occur is in the point in the spin axis, intersecting $\mathcal{S}_{ib}$ with angular momentum magnitude lower than the target $\|\overline{h}\|$, and with $s\|h\| = -\overline{h}$. In this case, since $h^* || s^*$:

$$
\beta = \frac{\|\mu_b\|}{\|\mu_i\|} = \frac{\|b \times h^*\|}{\|b \times s^*\|} = \frac{\|b\|\|h^*\|\cos\theta}{\|b\|\|s^*\|\cos\theta} = \frac{\|h^*\|}{\|s^*\|}, \tag{33}
$$

then with s^* and h^* in opposing directions, the point $x = \begin{bmatrix}(1 - \text{tol}_{ss})\overline{h}^T & -a^T\end{bmatrix}^T$ forms a local equilibrium. If the equilibrium is attractive, it can compromise the convergence of the system to the target equilibrium. From the results of the numerical simulations presented in Section 4, this local equilibrium is not expected to affect the asymptotic stability of the target partial equilibrium $s^* = 0$, but rigorous proof of its behavior is left to future work.

ACKNOWLEDGMENTS

This work was supported by NASA's Space Technology Mission Directorate (STMD) Small Satellite Technology Program (SSTP) under NASA Grant Number 80NSSC21K0446. This work was partially supported by Fundação para a Ciência e a Tecnologia (Portuguese Foundation for Science and Technology) through the Carnegie Mellon Portugal Program under fellowship PRT/BD/154921/2022.

REFERENCES

[1] M. Y. Ovchinnikov and D. Roldugin, "A survey on active magnetic attitude control algorithms for small satellites," *Progress in Aerospace Sciences*, vol. 109, p. 100546, Aug. 2019. [Online]. Available: https://linkinghub.elsevier.com/retrieve/pii/S0376042119300569

[2] L. He, W. Ma, P. Guo, and T. Sheng, "Developments of attitude determination and control system of microsats: A survey," *Proceedings of the Institution of Mechanical Engineers, Part I: Journal of Systems and Control Engineering*, vol. 235, no. 10, pp. 1733–1750, Nov. 2021. [Online]. Available: http://journals.sagepub.com/doi/10.1177/0959651819895173

[3] Z. Manchester, "Lyapunov-based control for flat-spin recovery and spin inversion of spin-stabilized spacecraft," in *AIAA/AAS Astrodynamics Specialist Conference*, 2016, p. 5644.

[4] G. Avanzini, E. De Angelis, and F. Giulietti, "Spin-axis pointing of a magnetically actuated spacecraft," *Acta Astronautica*, vol. 94, no. 1, pp. 493–501, Jan. 2014. [Online]. Available: https://linkinghub.elsevier.com/retrieve/pii/S0094576512004249

[5] D. Roldugin and P. Testani, "Spin-stabilized satellite magnetic attitude control scheme without initial detumbling," *Acta Astronautica*, vol. 94, no. 1, pp. 446–454, Jan. 2014. [Online]. Available: https://linkinghub.elsevier.com/retrieve/pii/S0094576513000234

[6] N. Sugimura, T. Kuwahara, and K. Yoshida, "Attitude determination and control system for nadir pointing using magnetorquer and magnetometer," in *2016 IEEE Aerospace Conference*. Big Sky, MT, USA: IEEE, Mar. 2016, pp. 1–12. [Online]. Available: http://ieeexplore.ieee.org/document/7500665/

[7] J. Abbott, "Acquisition of sun-pointing attitude by space vehicles without the use of rate gyroscopes," in *Proceedings of the Institution of Electrical Engineers*, vol. 114, no. 10. IET, 1967, pp. 1577–1581.

[8] C. Chasset, R. Noteborn, P. Bodin, R. Larsson, and B. Jakobsson, "3-Axis magnetic control: flight results of the TANGO satellite in the PRISMA mission," *CEAS Space Journal*, vol. 5, no. 1-2, pp. 1–17, Sep. 2013. [Online]. Available: http://link.springer.com/10.1007/s12567-013-0034-9

[9] Y. He, Z. Wang, S. Yang, and W. He, "Sun-pointing safe control for atmospheric environment monitoring satellite using magnetic actuation," *Advances in Space Research*, vol. 72, no. 5, pp. 1528–1537, Sep. 2023. [Online]. Available: https://linkinghub.elsevier.com/retrieve/pii/S0273117723003228

[10] C. A. Sedlund, "A simple sun-pointing magnetic controller for satellites in equatorial orbits," in *2009 IEEE Aerospace conference*. Big Sky, MT, USA: IEEE, Mar. 2009, pp. 1–12. [Online]. Available: http://ieeexplore.ieee.org/document/4839544/

[11] A. Colagrossi and M. Lavagna, "A Spacecraft Attitude Determination and Control Algorithm for Solar Arrays Pointing Leveraging Sun Angle and Angular Rates Measurements," *Algorithms*, vol. 15, no. 2, p. 29, Jan. 2022. [Online]. Available: https://www.mdpi.com/1999-4893/15/2/29

[12] J. Kim and K. Worrall, "Sun tracking controller for UKube-1 using magnetic torquer only*," *IFAC Proceedings Volumes*, vol. 46, no. 19, pp. 541–546, 2013. [Online]. Available: https://linkinghub.elsevier.com/retrieve/pii/S1474667015363801

[13] M. Holliday, R. Ticknor, J. Stupl, R. Hunter, P. Fisch, I. S. Sow, J. Willis, and Z. Manchester, "The py4 mission: A low-cost demonstration of cubesat formation-flying technologies," 2024.

[14] T. R. Kane, P. W. Likins, D. A. Levinson *et al.*, *Spacecraft dynamics*. McGraw-Hill New York, 1983, vol. 1.

[15] J.-J. E. Slotine, W. Li *et al.*, *Applied nonlinear control*. Prentice hall Englewood Cliffs, NJ, 1991, vol. 199, no. 1.

[16] H. K. Khalil and J. W. Grizzle, *Nonlinear systems*. Prentice hall Upper Saddle River, NJ, 2002, vol. 3.

[17] D. Liberzon, *Switching in systems and control*. Springer, 2003, vol. 190.

[18] G. Avanzini and F. Giulietti, "Magnetic detumbling of a rigid spacecraft," *Journal of guidance, control, and dynamics*, vol. 35, no. 4, pp. 1326–1334, 2012.

[19] F. Blanchini, "Set invariance in control," *Automatica*, vol. 35, no. 11, pp. 1747–1767, 1999.

[20] J. Chai and R. G. Sanfelice, "On notions and sufficient conditions for forward invariance of sets for hybrid dynamical systems," in *2015 54th IEEE Conference on Decision and Control (CDC)*. IEEE, 2015, pp. 2869–2874.

[21] W. Kutta, *Beitrag zur näherungsweisen Integration totaler Differentialgleichungen*. Teubner, 1901.

[22] P. C. Hughes, *Spacecraft attitude dynamics*. Courier Corporation, 2012.

[23] G. Avanzini, E. L. de Angelis, and F. Giulietti, "Acquisition of a desired pure-spin condition for a magnetically actuated spacecraft," *Journal of Guidance, Control, and Dynamics*, vol. 36, no. 6, pp. 1816–1821, 2013.

BIOGRAPHY

Paulo Fisch *is a PhD candidate in the Robotics Institute at Carnegie Mellon University. He has previous experience working at the German Aerospace Center (DLR) and got his Mechanical Engineering degree from the University of São Paulo in 2020. His interests include satellite Guidance and Navigation Systems, optimal control and state estimation for space systems, with recent work on satellite orbit determination.*

Pedro Cachim *received a dual M.S. in Aerospace Engineering from Instituto Superior Técnico and ISAE-SUPAERO in 2020 and worked as a GNC engineer at GMV. He is pursuing a dual degree PhD in Electrical and Computer Engineering between the University of Lisbon and Carnegie Mellon University. His research interests include navigation and control for aerospace applications.*

Max Holliday *builds embedded systems for harsh environments. Hardware, firmware, software. Participated in numerous successful on-orbit missions. Max has designed, built, and operated several small-spacecraft constellations in LEO. He got his PhD from Stanford University. He focused on device and system-level techniques for mitigating radiation-induced degradation of commercial-off-the-shelf electronic systems for space. Max is also the founder and maintainer of PyCubed, an open-source satellite platform used across the industry.*

Rodrigo Ventura *(PhD) is a tenured Associate Professor of the Electrical and Computer Engineering Department of Instituto Superior Técnico (IST), University of Lisbon, and a senior researcher of the Institute for Systems and Robotics (ISR-Lisbon). Broadly, his research is focused on the intersection between Robotics and Artificial Intelligence, with particular interest in aerospace applications.*

Pedro Lourenço *(PhD) is the head of the Advanced Guidance and Control section within the Flight Segment and Robotics unit of GMV, working on space rendezvous, reusable transportation systems, OSAM, AOCS, etc. As section head, he has led R&D&I efforts towards the adoption of robust and optimization-based G&C and its verification and validation.*

Zac Manchester *is an associate professor in the Robotics Institute at Carnegie Mellon University and founder of the Robotic Exploration Lab. He received a PhD in aerospace engineering in 2015 and a BS in applied physics in 2009, both from Cornell University. His research interests include control and optimization with application to aerospace and robotic systems with challenging nonlinear dynamics.*